Article:

Zhu, Z.Q. orcid.org/0000-0001-7175-3307 and Liu, Y. (2018) Analysis of air-gap field modulation and magnetic gearing effect in fractional slot concentrated winding permanent magnet synchronous machines. IEEE Transactions on Industrial Electronics, 65 (5). pp. 3688-3698. ISSN 0278-0046

https://doi.org/10.1109/TIE.2017.2758747

Analysis of Air-gap Field Modulation and Magnetic Gearing Effect in Fractional Slot Concentrated Winding Permanent Magnet Synchronous Machines

Z. Q. Zhu, *Fellow, IEEE,* and Yue Liu, *Student Member, IEEE*

***Abstract*—In this paper, the torque production of fractional slot concentrated winding (FSCW) permanent magnet synchronous machines (PMSM) are analyzed from the perspective of the air-gap field harmonics modulation accounting for slotting effect. It is found that the average torque of FSCW PMSM is produced by both the principle of conventional PMSM and the magnetic gearing effect. A finite element analysis (FEA)-based equivalent current sheet model and harmonic restoration method is firstly used in FSCW PM machines with different slot-pole number combinations to quantify the respective contribution of the conventional PMSM and the magnetic gearing effect to the average torque. The influence of slot opening on the magnetic gearing effect, cogging torque and torque ripple is analyzed. The results show that the magnetic gearing effect makes a non-ignorable contribution to the average torque when a large slot opening stator is used. The expression of the gear ratio in FSCW PMSMs is derived. The influence of gear ratio on the contribution of the magnetic gearing effect to the total torque is investigated by FEA. The FEA predicted torques are validated by experiments on the prototypes.**

***Index Terms*—concentrated winding, fractional slot, magnetic gear, magnetically geared machine, magnetic gearing effect, modulation, permanent magnet machines.**

I. Introduction

FRACTIONAL slot concentrated winding (FSCW) permanent magnet (PM) synchronous machines have been gaining popularities in academics and industries in the past few decades [1]. They have advantages of compact size, high efficiency, high torque density, low cogging torque and fault tolerance [1] [2]. Overviews of the research on FSCW PM machines can be found in [1] and [3].

Different from integral slot distributed winding machines which generally have more sinusoidal armature reaction flux density distributions, the FSCW machines have usually non-sinusoidal armature reaction flux density distributions in the air gap, which means there are abundant armature field harmonics in the air-gap magnetic field. When open or semi-closed slots are used together with fractional-slot windings, for a more accurate calculation, slotting effect should be taken into consideration. The influence of stator slotting on the air-gap flux density waveform may be accounted for by using relative permeance model [4] [5], complex permeance model [6] or subdomain model [7].

In the past years, the research of slot harmonics and modulation effect are mainly focused on parasitic effects such as cogging torque [8] [9], torque ripple [10], unbalanced magnetic force [11] [12], noise and vibration [13] [14]. The influence of slotting modulation on the PM and rotor iron losses have also been investigated in [15]-[17].

Recently, the modulation effect in electrical machines has drawn researchers' attention [18] mainly because the average torque can be produced by two magnetic field with different pole numbers after modulation. This phenomenon is termed as airgap field modulation and/or magnetic gearing effect, which has been proven to be the working principle of magnetic gear [19] and magnetic geared machines [20] such as Vernier [21] [22], flux-modulated [23] and switched flux (SF) [24] [25] machines. Although the slot harmonics and modulation effect has been researched extensively in FSCW PMSMs, the contribution of the modulation effect/magnetic gearing effect to the average torque has not been researched in FSCW PMSMs yet. The torque in FSCW PMSMs was believed to be produced by classical torque production principle of PM machines only.

The aim of this paper is to reveal the contribution of modulation effect to the average torque, i.e., the magnetic gearing effect in FSCW PMSMs. It contributes a non-ignorable part to the total torque especially when FSCW PMSMs have large slot openings. Since average electromagnetic torque is the most critical performance for PMSMs, this paper will analyze the torque production mechanism in depth. The contribution of magnetic gearing effect to the average electromagnetic torque can be quantified using the finite element analysis (FEA)-based equivalent current sheet model (ECSM) and a harmonic restoration method. The results reveal that the FSCW PMSM is a combination of a PM machine and a magnetic gear in terms of average torque production.

Manuscript received April 16, 2017; revised August 26, 2017; accepted September 13, 2017.
The authors are with the Department of Electronic and Electrical Engineering, University of Sheffield, Sheffield, UK. (e-mail: z.q.zhu@sheffield.ac.uk, yliu147@sheffield.ac.uk).

This paper is organized as follows. In section II, the general torque production mechanism of FSCW PM machines is investigated based on the air-gap flux harmonics modulation accounting for slotting effect. It is found that the average electromagnetic torque is produced via two principles: the conventional PMSM and the magnetic gearing effect. In section III, a FEA-based ECSM is employed for an 8-pole-12-slot FSCM PMSM to quantify the respective contribution of conventional slotless PMSM and magnetic gearing effect to the average electromagnetic torque. In section IV, the influence of slot opening on the magnetic gearing effect, cogging torque and torque ripple is analyzed. In section V, based on the former analysis, the expression of gear ratio is given in this paper. The influence of gear ratio on the contribution of the magnetic gearing effect to the average torque is investigated by FEA in a series of FSCW PMSMs. Finally, prototypes are manufactured to validate the FEA results.

II. Modulated Magnetic Field and Torque Production Analysis in FSCW PM Machines

In this section, the general PM and armature reaction air-gap magnetic fields of FSCW surface-mounted PM machines are derived. Their interaction and torque production mechanism will be given. To obtain an analytical model for the air-gap flux density, the discussion in this section is based on the following assumptions:

1) The permeance of the steel lamination is infinite and saturation is not considered. The aim of this section is focused on the modulating effect of the stator slots, viz., the modulated harmonic orders and speed of rotation but not on the actual amplitudes of the field harmonics. The tangential component of the air-gap magnetic field is, therefore, also neglected for simplicity.

2) The relative permeability of permanent magnets is equal to that of the air. The relative permeability of PM is very close to 1 and hence can be approximated.

3) The leakage flux and end effect are ignored for simplicity.

A. PM air-gap flux density

For a FSCW machine with surface mounted PMs, the magnetic motive force (MMF) generated by the PMs is shown in Fig. 1, and its Fourier series expansion Fr(θ,t) is given by (1).

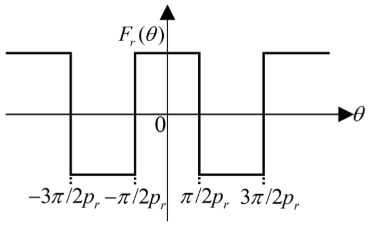

Fig. 1. MMF distribution generated by the PMs in FSCW machines.

$$F_r(\theta,t) = \sum_{i=1,3,5...}^{\infty} A_i \cos ip_r(\Omega_r t - \theta) \qquad (1)$$

where p_r is the number of the PM pole pairs, which is defined to be the fundamental harmonic of the FSCW PMSM in this paper, Ω_r is its mechanical rotating velocity, i is a positive odd integer, A_i is the amplitude of the ith order harmonic and θ is the air-gap circumferential position.

The air-gap permeance and the influence of slotting may be accounted for by introducing a permeance function shown in Fig. 2, in which θ_t is half-arc of a stator tooth.

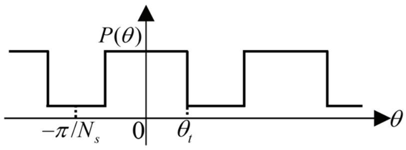

Fig. 2. Air-gap permeance function accounting for slotting effect.

And its Fourier series can be obtained as:

$$P(\theta) = \sum_{j=0,1,2...}^{\infty} P_j \cos(jN_s\theta) \qquad (2)$$

where N_s is the number of the stator tooth, j is either 0 or a positive integer, P_j is the amplitude of jth order harmonic.

Thus, the modulated PM air-gap flux density in the radial direction can be expressed as:

$$\begin{aligned} B_r &= F_r P \\ &= \frac{1}{2}\sum_{j=0,1,2...}^{\infty}\sum_{i=1,3,5...}^{\infty} A_i P_j \cos[ip_r\Omega_r t - (ip_r + jN_s)\theta] \\ &+ \frac{1}{2}\sum_{j=0,1,2...}^{\infty}\sum_{i=1,3,5...}^{\infty} A_i P_j \cos[ip_r\Omega_r t - (ip_r - jN_s)\theta] \end{aligned} \qquad (3)$$

From (3), the attributes of the modulated PM air-gap harmonics are given in Table I. After the modulation of stator slots, apart from the original harmonics of order ip_r with the mechanical speed of rotation of Ω_r, there also exist modulated harmonics with the order of $|ip_r \pm jN_s|$ rotating at the speed of $ip_r\Omega_r/(ip_r \pm jN_s)$. The positive and negative speed of rotations correspond to the harmonics rotating in the same or reverse direction with the rotor.

B. Armature reaction air-gap flux density

For a FSCW PM machine, the armature reaction MMF can be expressed as:

$$F_s(\theta,t) = \sum_{k}^{\infty} F_k \cos(\omega_s - k\theta) + \sum_{m}^{\infty} F_m \cos(-\omega_s - m\theta) \qquad (4)$$

where ω_s is its electrical rotating velocity, $\omega_s = p_r\Omega_r$, m and k are positive integers depending on the distribution of stator windings, F_k and F_m are the amplitudes of the kth and the mth order harmonics.

Similarly, the modulated armature reaction air-gap flux density in the radial direction can be deduced by multiplying $F_s(\theta,t)$ and $P(\theta)$ from (4) and (2), the attributes of the modulated armature reaction air-gap field flux harmonics are given in Table II. It can be seen that apart from the original kth (or mth) armature reaction magnetic field harmonic with the mechanical speed of rotation of $p_r\Omega_r/k$ (or $-p_r\Omega_r/m$), there also exist modulated harmonics with the order of $|k(m) \pm jN_s|$ rotating at the mechanical speed of $p_r\Omega_r/(k \pm jN_s)$ (or $-p_r\Omega_r/(m \pm jN_s)$).

C. Interaction of air-gap magnetic field harmonics

Based on the classical electromagnetic theory, there are three conditions for torque production between two magnetic field harmonics, which are summarized as follows:

This article has been accepted for publication in a future issue of this journal, but has not been fully edited. Content may change prior to final publication. Citation information: DOI 10.1109/TIE.2017.2758747, IEEE Transactions on Industrial Electronics

(a) They have the same pole pairs and speed, and then produce steady torque. In this case, there are two possible cases which are listed as follows:

(a-1) The two magnetic fields have the same pole-pair and speed, they can interaction with each other directly and produce steady torque as shown in Fig. 3(a). This was believed to be the principle of the conventional PMSMs such as FSCW PMSMs.

(a-2) The two magnetic fields have different pole-pairs and mechanical speed of rotations. However, there are flux modulation poles (FMPs) between them, and steady torque can still be produced if the two magnetic fields have the same frequency and their pole-pair numbers, satisfying:

$$p_h = N_f \pm p_l \quad (5)$$

where p_l is the pole-pair number of the low-speed magnetic field and p_h is the pole-pair number of the high-speed magnetic field. N_f it the pole number of FMPs. This phenomenon is termed as airgap field modulation and/or magnetic gearing effect, i.e. field modulation effect from the view point of airgap field and magnetic gearing effect from the view point of torque production. Fig. 3 (b) shows a schematic of magnetic gearing effect. The FMPs can modulate the magnetic fields and make them have the same pole-pair number and speed of rotation in the corresponding air-gap to produce steady torque. The gear ratio, which is the ratio of speeds of rotation between two magnetic fields, is given by:

$$G_r = \frac{p_h}{p_l} \quad (6)$$

Table III shows the attributes of magnetic gearing effect. Since p_l is larger than p_h as shown in Fig. 3(b), it can be seen that the low speed field can have an increased torque at a reduced speed. The torque production principle of magnetic gearing effect has drawn researchers' attention because of this reason and has been proven to be the working principle of high torque density magnetic gears [19]. Moreover, the contribution of magnetic gearing effect to the torque production have also been investigated widely in of Vernier, flux-modulated and switched flux (SF) machines [20]-[26].

(b) They have the same pole pairs but different speed, and then produce torque ripples;

(c) The pole pairs of the two harmonics are different, and they will produce no torque.

TABLE I
ATTRIBUTES OF MODULATED PM FIELD HARMONICS

Harmonic order	Mechanical speed of rotation
$\lvert ip_r \pm jN_s \rvert$	$\frac{ip_r\Omega_r}{ip_r \pm jN_s}$

TABLE II
ATTRIBUTES OF MODULATED ARMATURE REACTION FIELD HARMONICS

Harmonic order	Mechanical speed of rotation	Harmonic order	Mechanical speed of rotation
$\lvert k \pm jN_s \rvert$	$\frac{p_r\Omega_r}{k \pm jN_s}$	$\lvert m \pm jN_s \rvert$	$\frac{-p_r\Omega_r}{m \pm jN_s}$

TABLE III
ATTRIBUTES OF MAGNETIC GEARING EFFECT

	Pole pair number	Speed of rotation	Torque
High speed field	p_h	$n_r \cdot G_r$	T
Low speed field	p_l	n_r	$T \cdot G_r$

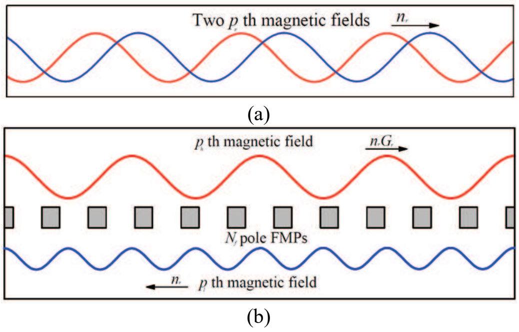

Fig. 3. Schematic of torque production mechanism. (a) Principle of conventional PM machines (a-1). (b) Principle of magnetic gearing effect (a-2).

D. Torque production mechanisms in FSCW PMSM

According to the analysis above, in a FSCW PM machine, the following equations must be satisfied to produce steady torque:

$$\begin{cases} \lvert ip_r \pm nN_s \rvert = \lvert k \pm jN_s \rvert \\ \dfrac{ip_r\Omega_r}{ip_r \pm nN_s} = \dfrac{p_r\Omega_r}{k \pm jN_s} \text{ or } \dfrac{-p_r\Omega_r}{m \pm jN_s} \end{cases} \quad (7)$$

where n is either 0 or a positive integer.

This means

$$\begin{cases} p_r = k & \text{Principle of conventional PM machines (8-a)} \\ p_r = \lvert k \pm jN_s \rvert & \text{Magnetic gearing effect (8-b)} \end{cases} \quad (8)$$

From (8), it is clear that the steady torque of FSCW PMSM can be generated from two main mechanisms:

(8-a) $p_r=k$: the fundamental open-circuit air-gap flux density harmonic and the unmodulated armature reaction harmonic share the same order and speed of rotation, they can interact with each other and produce useful torque. In this way, the torque is produced by the principle of the conventional PMSM.

(8-b) $p_r \neq k$: the $p_r th$ PM air-gap flux density harmonic and the kth armature reaction harmonic do not share the same order or speed of rotation, however, they have the same frequency ($p_r\Omega_r$) as shown in Table I and II. Hence, they can still interact with each other and produce steady torque under the modulation of air-gap permeance of order jN_s as long as they satisfy (8-b).

It is noteworthy that in FSCW PMSMs with p_r pole pairs of rotor PMs, due to the winding distribution, there exists armature reaction harmonic of order N_s-p_r and it has the same frequency with the $p_r th$ PM air-gap flux density harmonic, which satisfies (8-b). In this way, the torque in FSCW PMSMs can be produced by the magnetic gearing effect. The PM and armature reaction air-gap flux density harmonics play the role of the two magnetic fields, and the N_s pole stator tooth and slots play the role of FMPs. However, the magnetic gearing effect in FSCW PMSMs was ignored in the previous papers.

It should be noted that for FSCW PMSMs injected with sine wave current, only the $p_r th$ PM field harmonic is the working harmonic in the air-gap [18] [27]. Hence, the magnetic gearing effect in FSCW PMSMs can be further described as: the armature reaction harmonic is modulated to the fundamental order by the stator slots, it can interact with the fundamental PM harmonic and produce steady torque.

This article has been accepted for publication in a future issue of this journal, but has not been fully edited. Content may change prior to final publication. Citation information: DOI 10.1109/TIE.2017.2758747, IEEE Transactions on Industrial Electronics

Hence, it can be seen that the torque output of FSCW PMSM is not only produced by the principle of conventional PMSM but also by the magnetic gearing effect. The contribution of magnetic gearing effect to torque is highlighted and will be firstly quantified in this paper.

E. FE validation

In this section, an 8-pole-12-slot surface-mounted PM synchronous machine with open slots is used to validate the former theoretical analysis. The main design parameters of the machine are listed in Table VI. A 1/4 model of the 8-pole-12-slot machine is shown in Fig. 4.

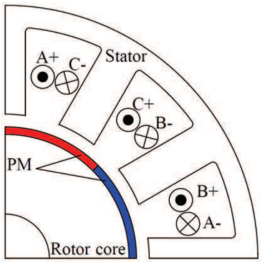

Fig. 4. ¼ model of an 8-pole-12-slot PM machine.

To validate (8), the torque produced by each air-gap magnetic flux density harmonic need to be identified. The air-gap magnetic flux density radial component B_r and tangential component B_t can be expanded by Fourier series:

$$\begin{cases} B_r(t,\theta) = \sum_k B_{rk}\cos(k\theta - \theta_{rk}) \\ B_t(t,\theta) = \sum_k B_{tk}\cos(k\theta - \theta_{tk}) \end{cases} \quad (9)$$

where B_{rk} and B_{tk} are the kth Fourier coefficients of B_r and B_t, θ_{rk} and θ_{tk} are their respective phases.

The electromagnetic torque produced by the kth radial and tangential airgap field flux harmonics can be derived by [28]:

$$T_k(t) = \frac{\pi r^2 l_{ef}}{\mu_0} B_{rk} B_{tk} \cos(\theta_{rk} - \theta_{tk}) \quad (10)$$

where r is the air-gap radius, μ_0 is the vacuum permeability, l_{ef} is the effective axial length. It is noteworthy that (10) is a general equation that can be used for either cogging torque or on-load torque.

The contribution of each air-gap harmonic to the torque can be obtained by combining FEA results and (10) as follows. At a certain time in an electrical period, the FE predicted B_r and B_t are expanded to the Fourier series based on (9). Hence, the value of B_{rk}, B_{tk}, θ_{rk} and θ_{tk} can be obtained. After this, the contribution of individual air-gap field harmonics to torque production at any time instant within the period can be quantified by (10) [28]. After repeating the above procedures over an electrical period, the average torque produced by the kth field harmonic within the full electric period can be obtained.

The cogging torque and on-load torque (the machine is fed with sinusoidal currents with the maximum phase current I_{max}=5A and operating under I_d=0 control) are calculated in FEA and the results are provided in Fig. 5 (a). For the cogging toque, the contribution of each air-gap magnetic flux density harmonic is calculated using (10) at the maximum value point which is 36 electrical degrees. The result is shown in Fig.5 (b). It can be seen that the 20th harmonic makes the most contribution to the cogging torque whereas the 28th harmonic has a negative effect on it. For the on-load torque in this 8-pole-12-slot machine, the torque ripple is mainly determined by the cogging torque as shown in Fig.5 (a). Hence, the 4th, 20th and 28th harmonics are taken as an example to investigate the variations of air-gap space harmonics with respect to the rotor position. The amplitudes, the cosine values of the phase difference of their radial and tangential components over an electrical period are shown in Fig. 5 (c) - (e). The instant contribution of each air-gap magnetic flux density harmonic to the instant torque are calculated by (10) at each time instant and shown in Fig. 5 (f). The average on-load torque produced by each air-gap harmonic within an electrical period is also calculated and the result is given by legend "Total" in Fig. 12. It shows that only the 4th air-gap magnetic flux density harmonic contributes to the total torque. For other harmonics such as 20th and 28th air-gap magnetic flux density harmonics, the average value of cos(θ_{rk} -θ_{tk}) in (9) is 0 in an electrical period as shown in Fig. 5 (e). Since the 4th harmonic is the fundamental harmonic in this machine, this means no useful torque will be produced by other harmonics except the fundamental harmonic, which validates the conclusion drawn from (9) that only p_rth PM air-gap flux density harmonic is the working harmonic. However, it is still unclear how much contribution the magnetic gearing effect makes to the average torque, i.e., to decompose the torque according to different torque production mechanisms shown in (8), which will be revealed in the next section.

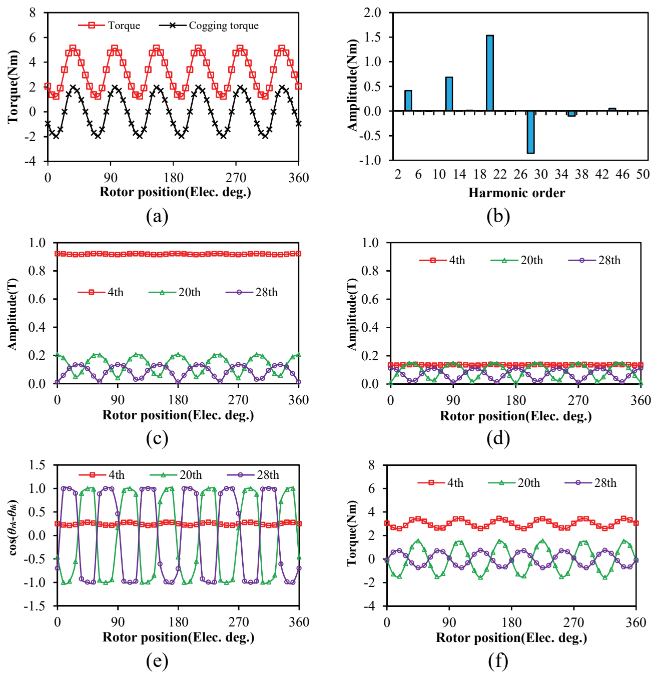

Fig. 5. FEA-predicted torque performance. (a) Waveforms of on-load torque and cogging torque. (b) Torque contribution of magnetic flux harmonics to the cogging torque. (c) Amplitude of radial component of air-gap magnetic flux density harmonics vs rotor position. (d) Amplitude of tangential component of air-gap magnetic flux density harmonics vs rotor position. (e) Variation of cos(θ_{rk} -θ_{tk}). (f) Instant torque contribution of individual air-gap flux density harmonics.

This article has been accepted for publication in a future issue of this journal, but has not been fully edited. Content may change prior to final publication. Citation information: DOI 10.1109/TIE.2017.2758747, IEEE Transactions on Industrial Electronics

III. Magnetic Gearing Effect in 8-Pole-12-Slot FSCW PMSM

A. Introduction of the FEA-based ECSM

In this subsection, an FEA-based equivalent current sheet (ECSM), which is the application of equivalent current sheet [29] [30] in FEA, is used to study the harmonic behavior under the modulation of stator slots, Fig. 6. The ECSM is a method in which the winding currents are approximated by an equivalent current sheet of infinitesimal thickness distributed over the stator slot openings. This method is used to be applied to analytical derivation of air-gap flux density harmonics [29] [30]. The FEA-base ECSM is to build an ECSM in the FEA software. Similar as the conventional ECSM in analytical method, in the FEA-based ECSM, the coils are wound in the same manner with the 8-pole-12-slot PM machine shown in Fig. 4. The thickness of the equivalent current sheet is designed very small compared to the air-gap length.

The armature reaction flux lines of the model in Fig. 4 and its FEA-Based ECSM in Fig. 6 are given in Fig. 7. It can be seen that the 8-pole-12-slot model and its FEA-based ECSM have the same main flux, the only difference between them is that the 8-pole-12-slot model has slot opening leakage flux whereas its FEA-based ECSM does not due to different position of coils.

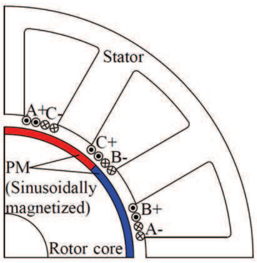

Fig. 6. ECSM of the 8-pole-12-slot machine.

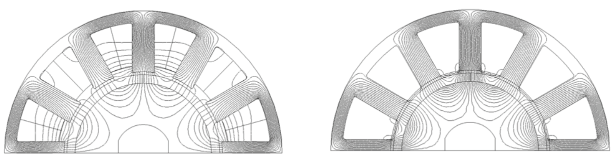

(a) (b)

Fig. 7. Armature reaction flux lines (I_a=5A, I_b=I_c=-2.5). (a) 8-pole-12-slot model. (b) FEA-based ECSM.

Since only the fundamental harmonic contributes to the average torque [18], the amplitude and phase of the 4th harmonic, which is the fundamental harmonic in 8-pole-12-slot machine, is given in Table IV. It can be seen that although the amplitudes of the corresponding harmonics in different models are not the same, the harmonics of the same order are in phase. To calibrate the difference in the amplitude caused by the position of the coils, the calibration coefficient k_c is introduced as:

$$k_c = \frac{A_V}{A_E} \tag{11}$$

where A_V and A_E are the amplitude of the fundamental harmonics in the FSCW PMSM and its FEA-based ECSM, respectively.

Hence, the amplitude of the 3-phase current I_E in FEA-based ECSM is set to be:

$$I_E = I_{max} k_c \tag{12}$$

TABLE IV
Amplitude and Phase of the 4th Harmonic

	8-pole-12-slot model		FEA-based ECSM	
	Radial	Tangential	Radial	Tangential
Amplitude(T)	0.054	0.023	0.051	0.021
Phase(°)	0	-90	-0	-90

B. Quantification of torque contribution in an 8-pole-12-slot machine

As has been analyzed and validated in Section II, the magnetic gearing effect only exists if the armature reaction harmonic of certain order is modulated to the fundamental order by the stator slots. Hence, it is important to have the information of each armature reaction harmonic before and after stator slotting modulation. However, all the armature reaction harmonics are from the same current excitation and cannot be separated once the current is injected. In this section, a harmonic restoration method is used to analyze the behavior of each armature reaction harmonic individually.

From FEA-based ECSM, a model without PMs and stator slots is firstly built to gain the information of the armature reaction harmonics before being modulated by stator slots, Fig. 8. The spectra and phases of the armature reaction air-gap magnetic flux density before modulation are calculated by FEA and shown in Fig. 9. According to Fig. 9, the amplitudes of the 4th, 8th and 20th harmonics are larger than the other harmonics. Moreover, since they satisfy (8), they are considered as priorities.

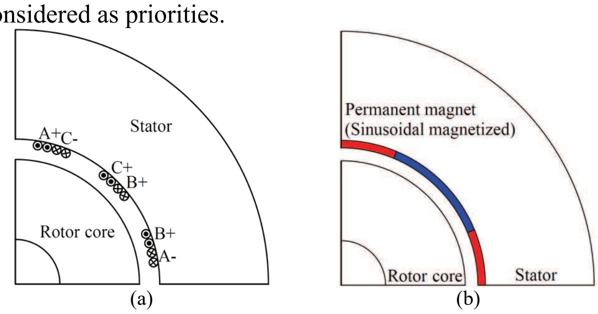

Fig. 8. Simulation of fields without modulation. (a) A model without PMs and stator slots. (b) Simulation of 4th armature reaction magnetic field by PMs.

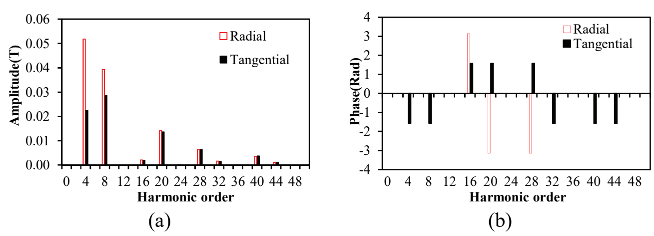

(a) (b)

Fig. 9. FE predicted armature reaction air-gap radial and tangential magnetic flux density harmonics before modulated. (a) Spectra. (b). Phases.

To analyze the behavior of the armature reaction magnetic flux density harmonic individually, it needs to be restored by the following way: an 8-pole outer rotor which consists of sinusoidally magnetized permanent magnets are built, which are shown in Fig. 8 (b). The thickness of the PMs is the same

This article has been accepted for publication in a future issue of this journal, but has not been fully edited. Content may change prior to final publication. Citation information: DOI 10.1109/TIE.2017.2758747, IEEE Transactions on Industrial Electronics

with that of the equivalent current sheet in Fig. 6. The remanence and the initial angle of the permanent magnets are adjusted so that the amplitude and phase of the 4th harmonic produced by outer PMs are the same with those by the armature reaction field before modulation. Similarly, a 16-pole outer rotor consists of sinusoidally magnetized permanent magnets are also built to simulate the 8th armature reaction field before being modulated by stator slotting.

After restoring the information of the armature reaction harmonics before modulation, their behavior under modulation effects can be seen in the following way: the interactions between the 4th PM field and the 4th and 8th armature reaction fields under the modulation effect are shown in Fig. 10. An 8-pole inner rotor, which is identical to the rotor in Fig. 6, is used to interact with the outer PMs. According to Table I-II, in Fig. 10 (a), both of the inner and outer PMs are rotating in the same direction at the mechanical speed n_r, whereas in Fig.10 (b), the 16-pole outer PMs rotate at half mechanical speed of the 8-pole inner rotor, in the opposite direction. Considering the slotting effect, the torque produced by each air gap field harmonic is calculated by (10) over an electrical period and the results are shown in Fig. 11.

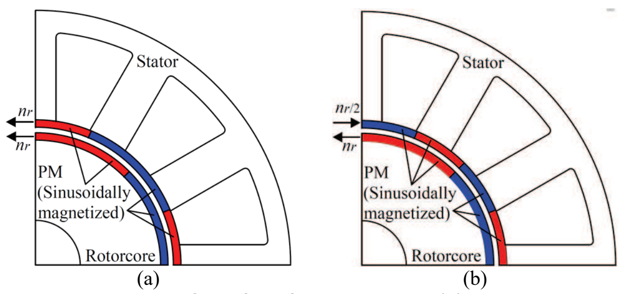

Fig. 10. Interaction of the field flux harmonics. (a) 4th PM MMF and 4th armature reaction MMF. (b) 4th PM MMF and 8th armature reaction MMF.

In Fig. 11, the torque produced by the interaction of magnetic fields Fig. 10 (a) is shown by legend "PMSM". Since the armature reaction and PM magnetic fields share the same order in this case, the torque component is produced by the principle of the conventional electrical machine. The torque produced by the interaction of magnetic fields in Fig. 10 (b) is illustrated by legend "MG". Since the 8th armature reaction and the 4th open-circuit magnetic fields do not share the same order, the torque component in this case is produced by the principle of the magnetic gearing effect, viz, the 8th armature reaction and 4th open-circuit magnetic fields can produce steady torque with the modulation effect of 12th air-gap permeance. In fact, Fig. 10 (b) is a magnetic gear with 8-pole inner rotor, 16-pole outer rotor and 12-pole iron pieces.

The accumulated result of the torque produced by the principle of conventional PMSM and magnetic gearing effect is given and compared with the total torque in Fig. 11. It can be seen that the accumulated result makes up >99% of the average torque, in which the magnetic gearing effect contributes 9.37% and the conventional PM machine principle contributes 89.63%. From this perspective, the FSCW PMSM can be regarded as a combination of conventional slotless PMSM and a magnetic gear.

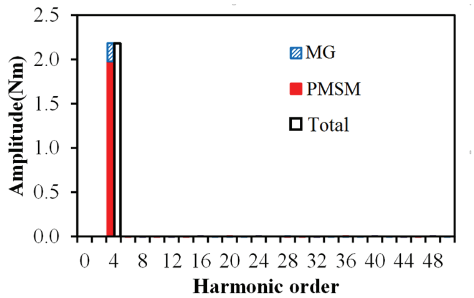

Fig. 11. Torque quantification.

IV. Influence of Slot Opening on Magnetic Gearing Effect

Since the slotting effect is the main cause of gearing effect in FSCW PMSMs, the influence of stator slot opening on the field harmonics and the contribution of gearing effect to the average torque are investigated in this section. The amplitudes of the 4th armature reaction and the PM radial air-gap magnetic flux density harmonics and average torque with respect to different slot opening angles for the 8-pole-12-slot machine are provided in Figs. 12 and 13.

By adopting the FEA-based ECSM and the harmonic restoration method, the modulated 4th armature reaction air-gap magnetic flux density harmonic which is originated from the 8th armature reaction MMF and the unmodulated 4th armature reaction air-gap magnetic flux density harmonic which is originated from the 4th armature reaction MMF can be separated, as shown in Fig. 12 (a). It shows that the modulated 4th armature reaction air-gap magnetic flux density harmonic increases with the increase of slot opening.

In Fig. 12 (b), since the DC component of equivalent air-gap permeance increases with the decrease of slot opening, the amplitudes of fundamental harmonics increase with the decrease of slot opening. However, with the decrease of the slot opening, the tooth-tip leakage flux increases, and therefore, the amplitude of 4th armature reaction air-gap magnetic flux density harmonic as well as the average torque decreases when the slot opening is very small. The tangential PM and armature reaction air-gap flux density harmonics follow the same trend with the radial components.

The torque produced by the interaction of the modulated 4th armature reaction harmonic and PM harmonic is based on the principle of magnetic gearing, whereas the torque produced by the unmodulated 4th armature reaction harmonic and PM harmonic is based on the principle of conventional PMSM. Therefore, their respective contribution to the average electromagnetic torque can also be quantified, which is shown in Fig. 13 (a). It can be seen that with the increase of slot opening, the amplitude of modulated 4th armature reaction field harmonic increases, therefore, the contribution of magnetic gearing effect to the total torque increases.

To evaluate the contribution of the magnetic gearing effect to the average torque in an electrical machine, the ratio of the torque produced by the magnetic gearing effect to the total torque is employed:

$$\rho = \frac{T_m}{T_t} \tag{13}$$

This article has been accepted for publication in a future issue of this journal, but has not been fully edited. Content may change prior to final publication. Citation information: DOI 10.1109/TIE.2017.2758747, IEEE Transactions on Industrial Electronics

where T_m is the torque produced by the magnetic gearing effect, T_t is the average torque. The ratio ρ with respect to the slot opening angle for the 8-pole-12-slot machine is also illustrated in Fig. 13 (a). It shows that the magnetic gearing effect becomes stronger with the increase of the slot opening.

Since slotting effect also brings about parasitic effects, Fig. 13 (b) shows the influence of the slot opening on the cogging torque and torque ripple. For the 8-pole-12-slot machine investigated in this paper, the cogging torque is the main ripple source for the torque ripple. According to Fig. 5, the 20th open-circuit air-gap flux density harmonic makes the most contribution to the cogging torque whereas the 28th harmonic has a negative contribution on it. From Fig. 12 (a), it can be seen that with the increase of the slot opening, the amplitude of 20th harmonic increases because of modulation effect of stator slot whereas the amplitude of 28th decreases. This explains why the cogging torque increases with the increase of slot opening.

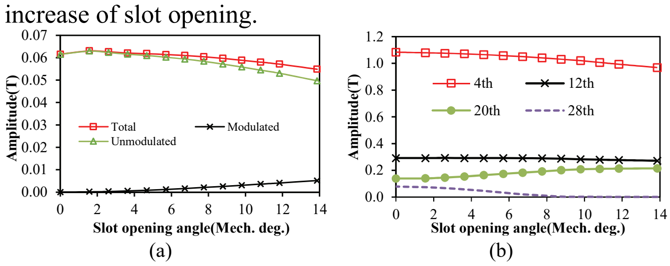

Fig. 12. Influence of slot opening on the field harmonics. (a) Armature reaction harmonics. (b) PM harmonics.

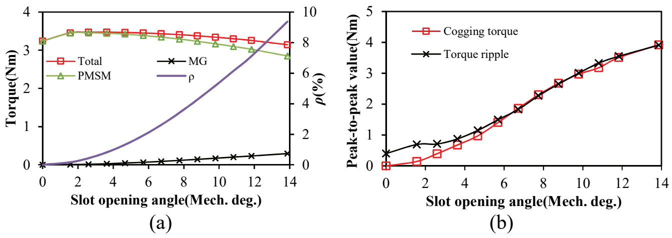

Fig. 13. Influence of slot opening on torque performance. (a) Average torque and torque contribution. (b) Cogging torque and torque ripple.

V. Gear Ratio and Magnetic Gearing Effect in Alternate FSCW PM Machines

In the 8-pole-12-slot PM machine, the 8th armature reaction magnetic field can interact with the 4th PM magnetic field under the modulation effect of stator slotting. The gear ratio, which is the ratio of speed between the high speed magnetic field and low speed magnetic field [19], is

$$G_r = \frac{-8}{4} = -2 \tag{14}$$

For FSCW PM machines with p_r pole pairs of rotor PMs, due to the winding distribution, the armature reaction harmonic of order N_s-p_r has a comparable amplitude with the fundamental p_rth armature reaction harmonic. With the speed of rotation of $-\omega_s/(N_s-p_r)$, the (N_s-p_r)th harmonic can form a magnetic gear with the fundamental open-circuit harmonic and stator tooth, making a contribution to the average torque.

Based on the analysis above, the gear ratio of the (N_s-p_r)th harmonic and the fundamental harmonic in FSCW PM machines can be defined as the ratio of their speed of rotation:

$$G_r = \frac{p_r - N_s}{p_r} \tag{15}$$

The contribution of gearing effect to the total torque output is also quantified in 6-pole-9-slot, 8-pole-9-slot, 10-pole-9-slot, 12-pole-9-slot, 10-pole-12-slot, 14-pole-12-slot and 16-pole-12-slot electrical machines with open slots. The stator geometry of the 12-slot and 9-slot machines are given in Fig. 14.

Fig. 14. Stator geometries. (a) 9-slot. (b) 12-slot.

The fundamental harmonics, the harmonics associated with magnetic gearing effect and gear ratios in the above FSCW PM machines are given in Table V.

TABLE V
Gear Ratios in FSCW PM Machines

N_s	p_r	N_s-p_r	G_r
12	4	8	-2
12	5	7	-7/5
12	7	5	-5/7
12	8	4	-1/2
9	4	5	-5/4
9	5	4	-4/5
9	3	6	-2
9	6	3	-1/2

The ratio ρ with respect to the gear ratio for different slot number are illustrated in Fig. 15. For the 8-pole-12-slot, 10-pole-12-slot, 14-pole-12-slot, 16-pole-12-slot, 6-pole-9-slot, 8-pole-9-slot, 10-pole-9-slot and 12-pole-9-slot FSCW PM machines, the intrinsic magnetic gearing effect contributes 9.37%, 9.97%, 12.8%, 14.7%, 14.3%, 16.9%, 20.9% and 23.1% to the total torque, respectively. It can be seen that for the same slot number, the magnetic gearing effect makes more contribution to the total torque with the increase of gear ratio, viz., for the same slot number, the magnetic gearing effect contributes more to the total torque when the rotor pole number is larger. The explanation is as follows. For the FSCW PMSM with a p_r pole pair rotor, the (N_s-p_r)th armature reaction harmonic exists in pair with the p_rth armature reaction harmonics, with comparable amplitude before modulation. The amplitude of (N_s-p_r)th armature reaction harmonic is larger if (N_s-p_r) is smaller than p_r. Therefore, with the increase of p_r, N_s-p_r decreases whereas its amplitude increases. In this way, it can contribute more to the average on-load torque after modulation.

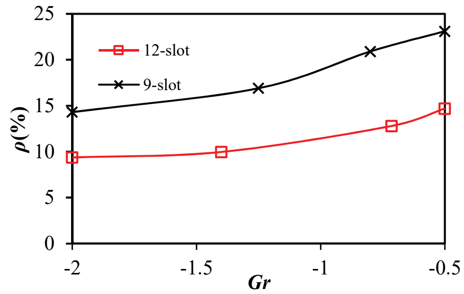

Fig. 15. Slot opening angle vs ρ in 9- and 12-slot machines.

This article has been accepted for publication in a future issue of this journal, but has not been fully edited. Content may change prior to final publication. Citation information: DOI 10.1109/TIE.2017.2758747, IEEE Transactions on Industrial Electronics

VI. Experimental Validation

The magnetic gearing effect and its contribution to the average torque in the foregoing sections cannot be measured directly on the prototypes because only the resultant torque waveform can be measured in the experiment. However, the influence of slot opening on torque can be validated by experiments. Hence, three 8-pole-12-slot machine prototypes with closed slot stator, semi-closed slot stator and open slot stator topologies are built, Figs. 16 (a)-(d). The dimensional parameters of the three prototypes are given in Table VI.

The experiments are implemented on the experimental setup shown in Fig. 16 (e) and (f). Fig. 16 (e) shows the machine drive units in which the inverters are controlled by the dSpace system and powered by the DC supply #1. In Fig. 16 (f), the prototypes are connected in tandem with the load machine and the dynamic torque is measured via the torque transducer. The test results will be displayed on the monitor and oscilloscope in Fig. 16 (e). The load machine is connected in series with DC supply #2 and an adjustable resistor to adjust the loading.

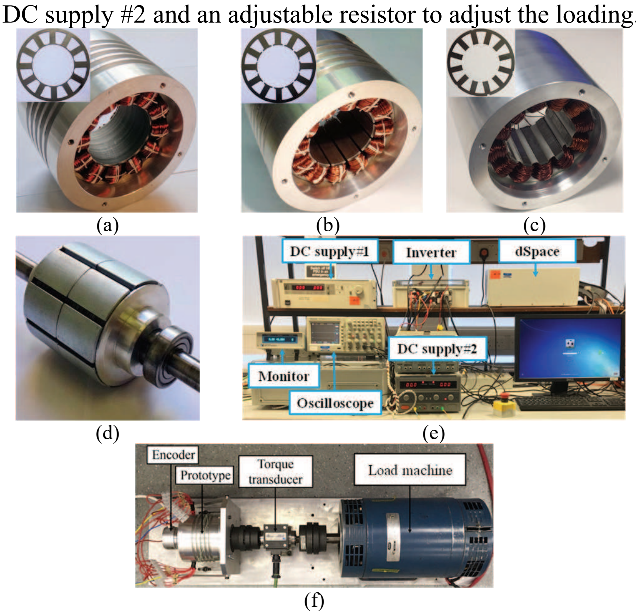

Fig. 16. Photos of prototypes and the test rig. (a) Closed-slot stator. (b) Semi-closed slot stator. (c) Open-slot stator. (d) Rotor. (e) Drive system. (f) Test rig.

TABLE VI
DIMENSIONAL PARAMETERS OF PROTOTYPES

Parameters	Closed	Semi-closed	Open
Slot/pole number	12/8		
Stator outer/inner diameter	100mm/57mm		
Rotor outer diameter	55mm		
Turns per phase	184		
PM thickness/ pole arc	3mm/155° Mech.		
Axial length	50mm		
Slot opening angle	0° Mech.	4° Mech.	14° Mech.

Fig. 17 compares the FEA and test results of the back-EMF waveforms and spectra. Fig. 18 compares the FEA and test results of the cogging torque and spectra. The measured torque waveforms are compared with the FEA results in Fig. 19. The waveforms are zoomed within 60 electric degrees because it is a torque ripple period for the 8-pole-12-slot PMSM, which is clearly shown in the spectra in Fig. 19 (d). Although 2-D FEA results are slightly higher than those of measurements due to end effect, friction, etc., good agreements are obtained. It also shows that the peak-to-peak value of cogging torque and the torque ripple increases with the increase of slot opening, which validates the correctness of the analysis.

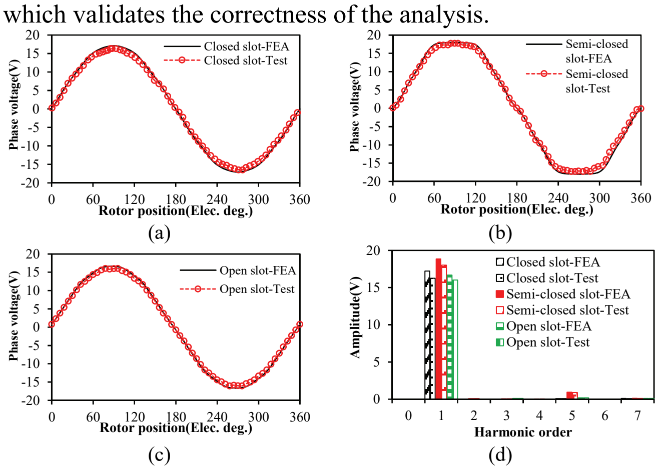

Fig. 17. Comparison of measured and predicted back EMF waveforms and spectra. (I_q=5A, I_d=0). (a) Closed-slot stator. (b) Semi-closed slot stator. (c) Open-slot stator. (d) Spectra.

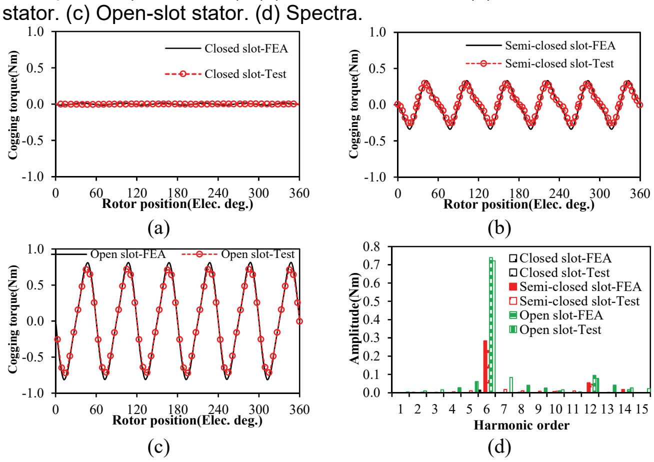

Fig. 18. Comparison of measured and predicted cogging torque waveforms and spectra. (I_q=5A, I_d=0). (a) Closed-slot stator. (b) Semi-closed slot stator. (c) Open-slot stator. (d) Spectra.

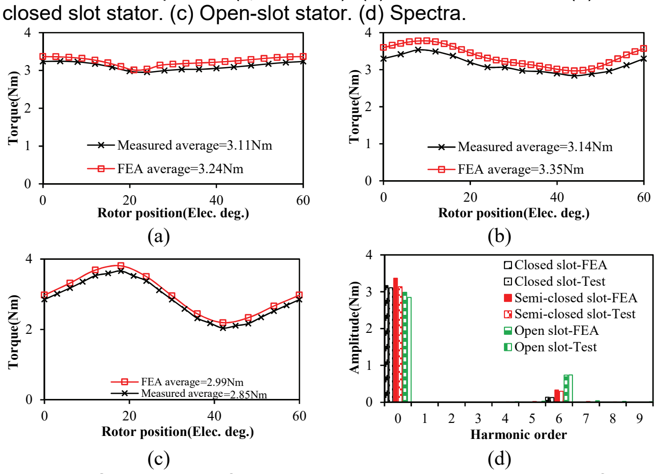

Fig. 19. Comparison of measured and predicted torque waveforms. (I_q=5A, I_d=0) (a) Closed-slot stator. (b) Semi-closed slot stator. (c) Open-slot stator. (d) Spectra.

VII. Conclusion

In this paper, the torque production mechanism of FSCW PMSMs is investigated from a new perspective, i.e. airgap field modulation and magnetic gearing effect. It is found that the FSCW PMSMs are working on both conventional PMSM principle and magnetic gearing effects. The respective contribution of the conventional PMSM and the magnetic gearing effect to the total torque is quantified by introducing a FEA-based ECSM and harmonic restoration method. The result shows that the contribution of the magnetic gearing effect is non-ignorable. The expression of the gear ratio in FSCW PMSMs is derived. The influence of gear ratio on the contribution of the magnetic gearing effect to the total torque is investigated. The influence of the slot opening on cogging torque and torque ripple is also investigated by FEA and validated by experiments.

REFERENCES

[1] A. M. EL-Refaie, "Fractional-slot concentrated-windings synchronous permanent magnet machines: Opportunities and challenges," *IEEE Trans. Ind. Electron.*, vol. 57, no. 1, pp. 107–121, Jan. 2010.

[2] D. Ishak, Z. Q. Zhu, and D. Howe, "Permanent magnet brushless machines with unequal tooth widths and similar slot and pole numbers," *IEEE Trans. Ind. Appl.*, vol. 41, no. 2, pp. 584–590, Mar./Apr. 2005.

[3] Z. Q. Zhu, "Fractional slot permanent magnet brushless machines and drives for electric and hybrid propulsion systems," *COMPEL - Int. J. Comput. Math. Electr. Electron. Eng.*, vol. 30, no. 1, pp. 9–31, 2011.

[4] Z. Q. Zhu and D. Howe, "Instantaneous magnetic field distribution in brushless permanent magnet dc motors. Part III: Effect of stator slotting," *IEEE Trans. Magn.*, vol. 29, no. 1, pp. 143–151, Jan. 1993.

[5] U. Kim and D. K. Lieu, "Magnetic field calculation in permanent magnet motors with rotor eccentricity: With slotting effect considered," *IEEE Trans. Magn.*, vol. 34, no. 4, pp. 2253–2266, Jul. 1998.

[6] D. Žarko, T. a Lipo, and D. Ban, "Analytical calculation of magnetic field distribution in the slotted air gap of a surface pm motor using complex relative air gap permeance," *IEEE Trans. Magn.*, vol. 42, no. 7, pp. 1828–1837, Jul. 2006.

[7] Z. Q. Zhu, L. J. Wu, and Z. P. Xia, "An accurate subdomain model for magnetic field computation in slotted surface-mounted permanent-magnet machines," *IEEE Trans. Magn.*, vol. 46, no. 4, pp. 1100–1115, Apr. 2010.

[8] L. Zhu, S. Z. Jiang, Z. Q. Zhu, and C. C. Chan, "Analytical methods for minimizing cogging torque in permanent-magnet machines," *IEEE Trans. Magn.*, vol. 45, no. 4, pp. 2023–2031, Apr. 2009.

[9] D. Zarko, D. Ban, and T. a. Lipo, "Analytical solution for cogging torque in surface permanent-magnet motors using conformal mapping," *IEEE Trans. Magn.*, vol. 44, no. 1, pp. 2943–2954, Jan. 2008.

[10] D. Zarko, D. Ban, and T. a. Lipo, "Analytical solution for electromagnetic torque in surface permanent-magnet motors using conformal mapping," *IEEE Trans. Magn.*, vol. 45, no. 7, pp. 2943–2954, Jul. 2009.

[11] G. Dajaku and D. Gerling, "The influence of permeance effect on the magnetic radial forces of permanent magnet synchronous machines," *IEEE Trans. Magn.*, vol. 49, no. 6, pp. 2953–2966, Jun. 2013.

[12] Z. Q. Zhu, Z. P. Xia, L. J. Wu, and G. W. Jewell, "Analytical modeling and finite-element computation of radial vibration force in fractional-slot permanent-magnet brushless machines," *IEEE Trans. Ind. Appl.*, vol. 46, no. 5, pp. 1908–1918, Sep./Oct. 2010.

[13] M. Valavi, S. Member, A. Nysveen, S. Member, R. Nilssen, and T. Rølvåg, "Slot harmonic effect on magnetic forces and vibration in low-speed permanent-magnet machine with concentrated windings," *IEEE Trans. Ind. Appl.*, vol. 50, no. 5, pp. 3304–3313, Sep./Oct. 2014.

[14] M. Fakam, M. Hecquet, V. Lanfranchi, and A. Randria, "Design and magnetic noise reduction of the surface permanent magnet synchronous machine using complex air-gap permeance," *IEEE Trans. Magn.*, vol. 51, no. 4, pp. 1–9, Apr. 2015.

[15] Z. X. Fang, Z. Q. Zhu, L. J. Wu, and Z. P. Xia, "Simple and accurate analytical estimation of slotting effect on magnet loss in fractional-slot surface-mounted PM machines," *in Proc. ICEM*, 2012, pp. 464–470.

[16] Juha Pyrhönen, H. Jussila, Y. Alexandrova, Pavol Rafajdus, and Janne Nerg, "Harmonic loss calculation in rotor surface permanent magnets—new analytic approach," *IEEE Trans. Magn.*, vol. 48, no. 8, pp. 2358–2366, Aug. 2012.

[17] E. Fornasiero, N. Bianchi, and S. Bolognani, "Slot harmonic impact on rotor losses in fractional-slot permanent-magnet machines," *IEEE Trans. Ind. Electron.*, vol. 59, no. 6, pp. 2557–2564, Jun. 2012.

[18] M. Cheng, P. Han, and W. Hua, "A general airgap field modulation theory for electrical machines," *IEEE Trans. Ind. Electron.*, DOI 10.1109/TIE.2017.2682792, 2017.

[19] K. Atallah, S. D. Calverley, and D. Howe, "Design, analysis and realisation of a high-performance magnetic gear," *IEE Proceedings-Electric Power Appl.*, vol. 151, no. 2, pp. 135–143, Feb. 2006..

[20] R. Qu, D. Li, and J. Wang, "Relationship between magnetic gears and Vernier PM machines," in Proc. Int. *Conf. Elect. Mach. Syst.*, Beijing, China, Aug. 18–20, 2011, pp. 1–6.

[21] D. Li, R. Qu, J. Li, L. Xiao, L. Wu, and W. Xu, "Analysis of torque capability and quality in Vernier permanent magnet machines," *IEEE Trans. Ind. Appl.*, vol. 52, no. 1, pp. 125–135, Jan./Feb. 2016.

[22] L. Wu, R. Qu, D. Li, and Y. Gao, "Influence of pole ratio and winding pole numbers on performance and optimal design parameters of surface permanent-magnet Vernier machines," *IEEE Trans. Ind. Appl.*, vol. 51, no. 5, pp. 3707–3715, Sep./Oct. 2015.

[23] J. M. Crider, and S. D. Sudhoff, "An inner rotor flux-modulated permanent magnet synchronous machine for low-speed high-torque applications," *IEEE Trans. Energy Convers.*, vol. 30, no. 3, pp. 1247–1254, Sep. 2015.

[24] Z. Z. Wu and Z. Q. Zhu, "Analysis of air-gap field modulation and magnetic gearing effects in switched flux permanent magnet machines," *IEEE Trans. Magn.*, vol. 51, no. 5, May 2015.

[25] Y. Shi, L. Jian, J. Wei, Z. Shao, W. Li, and C. C. Chan, "A new perspective on the operating principle of flux-switching permanent magnet machines," *IEEE Trans. Ind. Electron.*, vol. 63, no. 3, pp. 1425–1437, Mar. 2016.

[26] Y. Du, F. Xiao, W. Hua, X. Zhu, M. Cheng, L. Quan, and K. T. Chau, "Comparison of flux-switching PM motors with different winding configurations using magnetic gearing principle," *IEEE Trans. Magn.*, vol. 52, no. 5, May 2016.

[27] J. F. Cieras, C. Wang, and J. C. Lai, Noise of Polyphase Electric Motors. Boca Raton, FL: Taylor&Francis/CRC Press, 2006

[28] C. M. Spargo, B. C. Mecrow, and J. D. Widmer, "A seminumerical finite-element postprocessing torque ripple analysis technique for synchronous electric machines utilizing the air-gap Maxwell stress tensor," *IEEE Trans. Magn.*, vol. 50, no. 5, May 2014.

[29] D. Ishak, Z. Q. Zhu, and D. Howe, "Eddy-current loss in the rotor magnets of permanent-magnet brushless machines having a fractional number of slots per pole," *IEEE Trans. Magn.*, vol. 41, no. 9, pp. 2462–2469, Sep. 2005.

[30] K. F. Rasmussen, J. H. Davies, T. J. E. Miller, M. I. McGelp, and M. Olaru, "Analytical and numerical computation of air-gap magnetic fields in brushless motors with surface permanent magnets," *IEEE Trans. Ind. Appl.*, vol. 36, no. 6, pp. 1547–1554, 2000.

Z. Q. Zhu (M'90–SM'00–F'09) received the B.Eng. and M.Sc. degrees in electrical and electronic engineering from Zhejiang University, Hangzhou, China, in 1982 and 1984, respectively, and the Ph.D. degree in electronic and electrical engineering from The University of Sheffield, Sheffield, U.K., in 1991.

Since 1988, he has been with The University of Sheffield, where he currently holds the Royal Academy of Engineering/Siemens Research Chair and is the Head of the Electrical Machines and Drives Research Group, the Academic Director of Sheffield Siemens Wind Power Research Centre, the Director of CRRC Electric Drives Technology Research Centre, and the Director of Midea Electric Machines and Controls Research Centre. His current major research interests include the design and control of permanent-magnet brushless machines and drives for applications ranging from automotive through domestic appliances to renewable energy. He is a Fellow of Royal Academy of Engineering.

Yue Liu (S'16) received the B.Eng. and M.Sc. degrees in electrical and electronic engineering from Harbin Institute of Technology, Harbin, China, in 2013 and 2015, respectively. He is currently working toward the Ph.D. degree in the Department of Electronic and Electrical Engineering, University of Sheffield, Sheffield, U.K.